iScience

CellPress
OPEN ACCESS

Article

Proton conductivity of the protein-based velvet worm slime

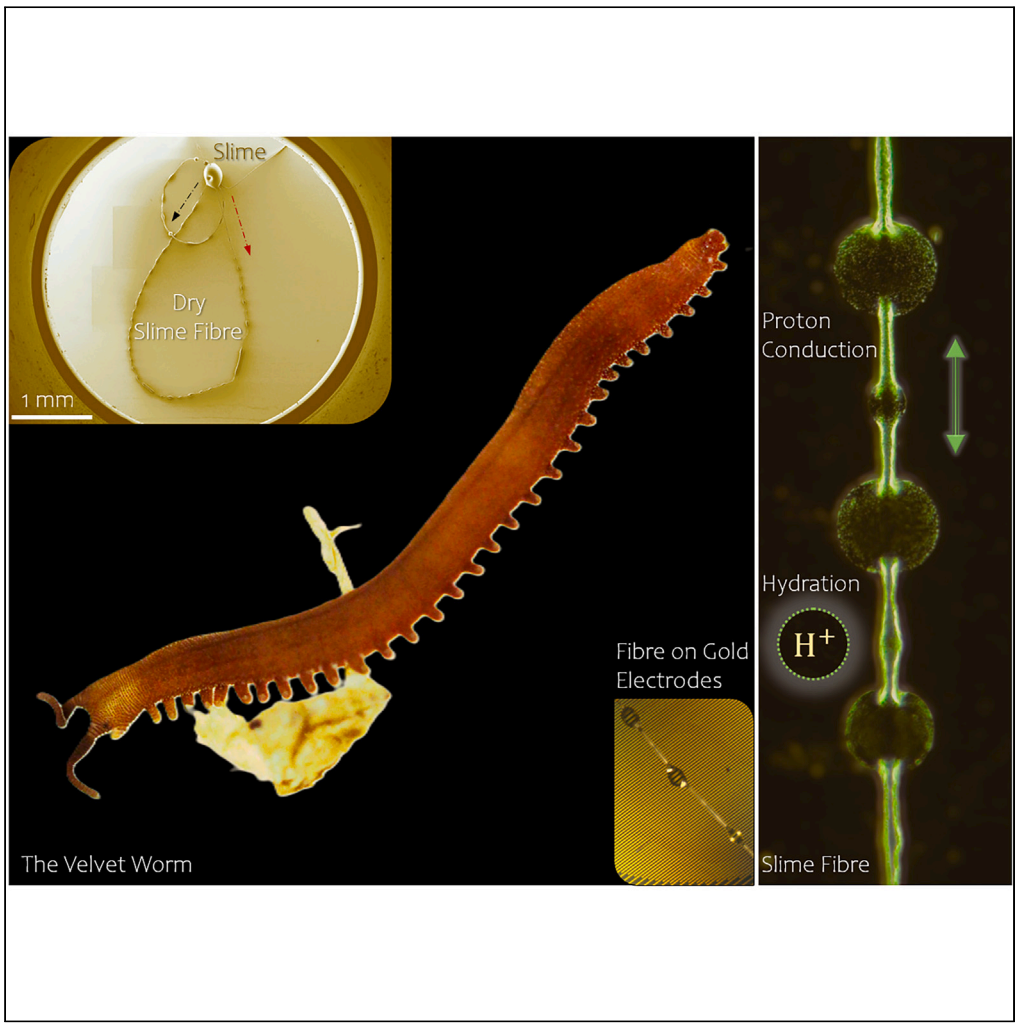

Rinku Saran, Maciej Klein, Bhargy Sharma, Jun Jie Loke, Quentin Moana Perrin, Ali Miserez

ali.miserez@ntu.edu.sg

Highlights

The slime of the velvet worm used for prey capture is a proton conducting material

The electrical conductivity of the slime depends on humidity, temperature, pH, and time

Electrical devices based on slime films and fibers are characterized

The slime proteins provide molecular design guidelines for bio-based proton conductors

Saran et al., iScience 27, 110216
July 19, 2024
https://doi.org/10.1016/j.isci.2024.110216

iScience

CellPress
OPEN ACCESS

Article

Proton conductivity of the protein-based velvet worm slime

Rinku Saran,[1] Maciej Klein,[2,3] Bhargy Sharma,[1] Jun Jie Loke,[1] Quentin Moana Perrin,[1] and Ali Miserez[1,4,5,*]

SUMMARY

The properties of complex bodily fluids are linked to their biological functions through natural selection. Velvet worms capture their prey by ensnaring them with a proteinaceous fluid (slime). We examined the electrical conductivity of slime and found that dry slime is an insulator. However, its conductivity can increase by up to 10^6 times in its hydrated state, which can be further increased by an order in magnitude under acidic hydration (pH $\approx$ 2.3). The transient current measured using ion-blocking electrodes showed a continuous decay for up to 7 h, revealing slime's nature as a proton conducting material. Slime undergoes a spontaneous fibrilization process producing high aspect ratio $\approx 10^5$ fibers that exhibit an average conductivity $\approx 2.4 \pm 1.1$ mS cm^{-1}. These findings enhance our understanding of slime as a natural biopolymer and provide molecular-level guidelines to rationally design biomaterials that may be employed as hygroscopic conductors.

INTRODUCTION

Onychophorans, commonly known as velvet worms, are cold-blooded organisms that have persisted on Earth since the early Cambrian period, surviving all mass extinctions.[1] There are more than 200 species that live in moist habitats. They breathe through open pores present along their soft hydrophobic skin and use multiple pairs of legs to undulate. Their vision is poor,[2] but they possess a series of sensory receptors spread all across their tactile spines, as well as a pair of antennae bearing mechano-chemoreceptive sensilla,[3] Figure 1A. Perhaps the most intriguing adaption of velvet worms is the use of their slime as a biochemical weapon to ensnare their prey. The slime is a transparent, viscous, and highly adhesive fluid squirted through worm's oral papillae in wavy oscillatory motion,[4] Figures 1A and 1B. The slime is produced within specialized glands, wherein it is stored as a viscous solution comprising 90% water. After being secreted by the worm, the slime swiftly solidifies upon contact with its prey; if subjected to shear stress, it transforms into long enmeshing fibers, Figure 1C. Upon drying, the residual mass of the slime mainly comprises of a multi-protein complex along with minute quantities of lipids.[5–7]

Over the past few years, the slime has been recognized as a biopolymer archetype because of its complex fluid mechanic characteristics.[8] The slime is composed of proteins that can undergo reversible liquid-to-solid transitions, viscoelastic gelation, surface adhesion, and stimulate fiber formation. The resulting fibers exhibit high tensile strength (102 MPa) and a Young's modulus of *ca.* 4.5 GPa in the dry state, on par with polyamide thermoplastics.[9] More importantly, the fibers are flexible, ductile, and recyclable i.e., they can be re-dissolved and regenerated again.[9–11] If mimicked synthetically, these attributes could generate a class of sustainable biopolymers with potential applications in manufacturing of reinforcing fibers, membranes, wet adhesives, bio-scaffolds, and implants. The prime aim of research on such complex biological fluids is to seek inspirations for material design and gain phylogenetic insights by investigating their physical properties. In this context, the velvet worm slime is of special interest because it is a proteinaceous material whose functional properties have been optimized through natural selection. To date, the electrical properties of the slime proteins are unknown, which we report in this work. Our findings provide evidence that slime is a proton conducting material in its hydrated state. The mechanism of proton conduction in biomaterials in their hydrated state has been reviewed recently.[12] Materials in which dominant electric current is carried out by protons rather than electrons are appealing for the development of solid-state protonic devices.

RESULTS AND DISCUSSION

Dependence of electrical conductivity on relative humidity and temperature

The electrical conductivity of slime was investigated by casting it as a solid-state film. Briefly, native slime squirted by the velvet worm upon gentle agitation was left to dry, followed by collection of dried solid flakes and their subsequent dissolution in water ($\approx$10–12 h). As prepared

[1]Biological and Biomimetic Material Laboratory, Centre for Sustainable Materials, School of Materials Science and Engineering, Nanyang Technological University, Singapore 639798, Singapore
[2]Centre for Disruptive Photonic Technologies, The Photonic Institute, Nanyang Technological University, 21 Nanyang Link, Singapore 637371, Singapore
[3]Division of Physics and Applied Physics, School of Physical and Mathematical Sciences, Nanyang Technological University, 21 Nanyang Link, Singapore 637371, Singapore
[4]School of Biological Sciences, Nanyang Technological University, Singapore 637551, Singapore
[5]Lead contact
*Correspondence: ali.miserez@ntu.edu.sg
https://doi.org/10.1016/j.isci.2024.110216

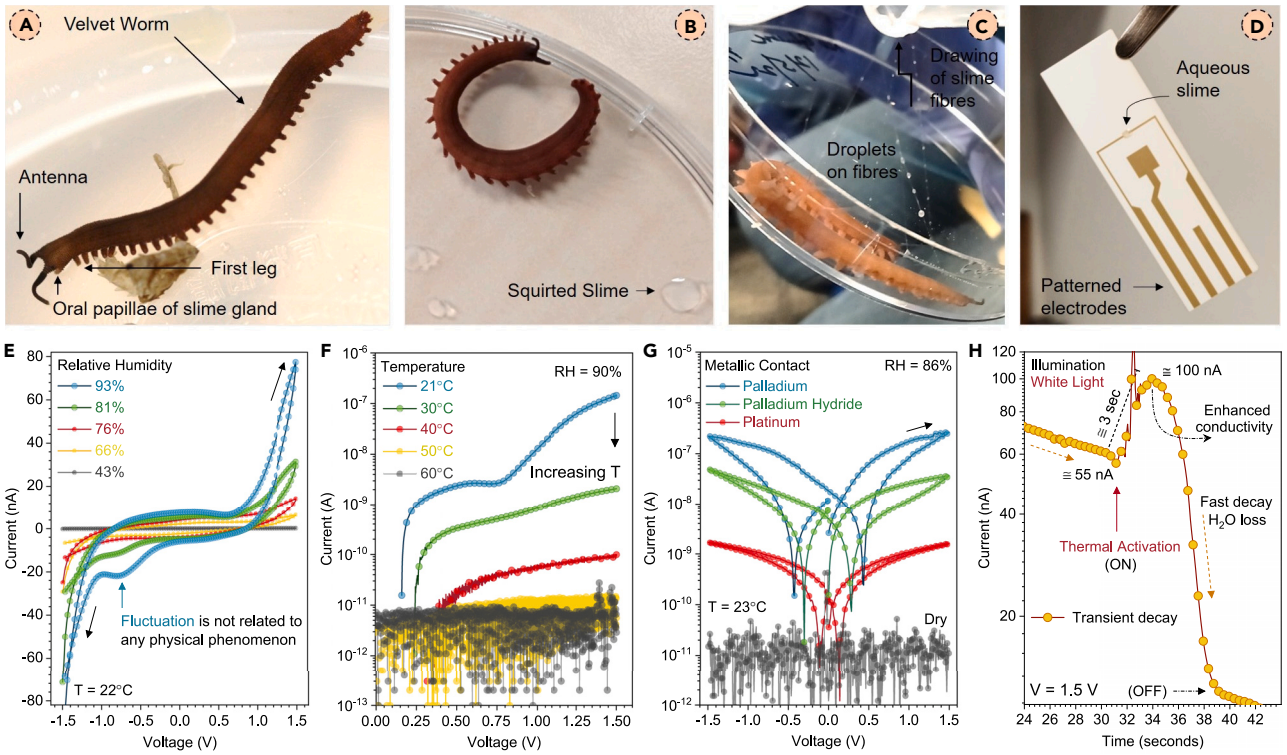

Figure 1. The slime of the velvet worm and its electrical characteristics

(A) Photograph of the Onychophoran species (Eoperipatus sp.) whose slime was used in this study.

(B) Photograph shows slime squirted by the worm from their oral papillae upon gentle agitation on its body.

(C) Photograph shows long slime fibers formed by mechanical drawing, fibers feature equally spaced droplets.

(D) Photograph of a typical electrical device fabricated by casting aqueous slime onto electrodes.

(E) Dependence of I-V characteristics on RH measured for the device shown in Figure 1D.

(F) Dependence of I-V characteristics on temperature at a constant RH level of 90%.

(G) Typical I-V characteristics of slime devices with Pt, Pd, and PdH_x contacts.

(H) Plot shows a sudden increase of the current as soon as the heat is applied to the slime device.

aqueous slime solutions (≈0.6–2.3 mg mL^{-1}) were drop casted (≈1–5 μL) to produce thin films, which were often air dried. We observe that electrical devices (Figure 1D) featuring a nitrogen dried slime film casted between metal electrodes did not conduct electricity. However, if the devices were kept under ambient conditions for a prolonged period, they allowed passage of a weak electric current. Therefore, to quantify this phenomenon, we recorded the current-voltage (I-V) characteristics of devices as a function of relative humidity (RH) and temperature (T). A strong dependence of electric current on RH levels between 43% and 93% was observed for a cyclic negative to positive voltage sweep (Figure 1E), which was five orders higher in magnitude relative to the dry film (Figure S1A).

We next recorded the I-V characteristics while keeping the device under a constant RH of 90% and then varying the temperature, Figure 1F. We observed that upon raising the device temperature from ≈21°C to 60°C, the current was reduced from ≈10^{-7}A to noise level, despite the fact that the device was being kept under 90% RH (Figure S1B). We suggest that a considerable loss of loosely bonded water molecules takes place upon raising the temperature from 21°C to 30°C or possibly a reduction in diffusivity of water molecules within the film (absorption) or viscosity. Upon lowering the temperature back to 21°C, the device regained its conductivity certifying that the temperature induced loss in conductivity was not permanent (Figure S1C), and that the hygroscopic properties of slime have a strong temperature dependence. Electronic, or ionic conductors, usually display an increase in conductivity over the temperature range (21°C–60°C)[13,14] because the electrical charge transport is a thermally activated process. We observed that the thermally activated charge transport in slime is a fast and likely a diffusion related process that occurs at T < 30°C in a very narrow T regime which we cannot determine precisely. To collectively demonstrate that the conductivity is hydration dependant and can be thermally activated, we measured the transient response of a hydrated film under light-induced heating (Figure 1H). Initially, the current slowly decayed from time (t) ≈ 0 s due to exposure of hydrated film to the ambient conditions. At t ≈ 30 s, the device was illuminated from top with a white light source (100 W) from a distance of 30 cm to induce heating that triggered the current to rapidly increase from ≈55 nA to ≈100 nA in less than 3 s. Following this, from t ≈ 34 s the current again starts to decay, at a much faster rate due to heat-induced dehydration. To further verify the thermally actuated enhancement and loss of conductivity at T ≥ 50°C, we measured the transient response of devices by keeping them under a constant humidity level and then applied thermal heating

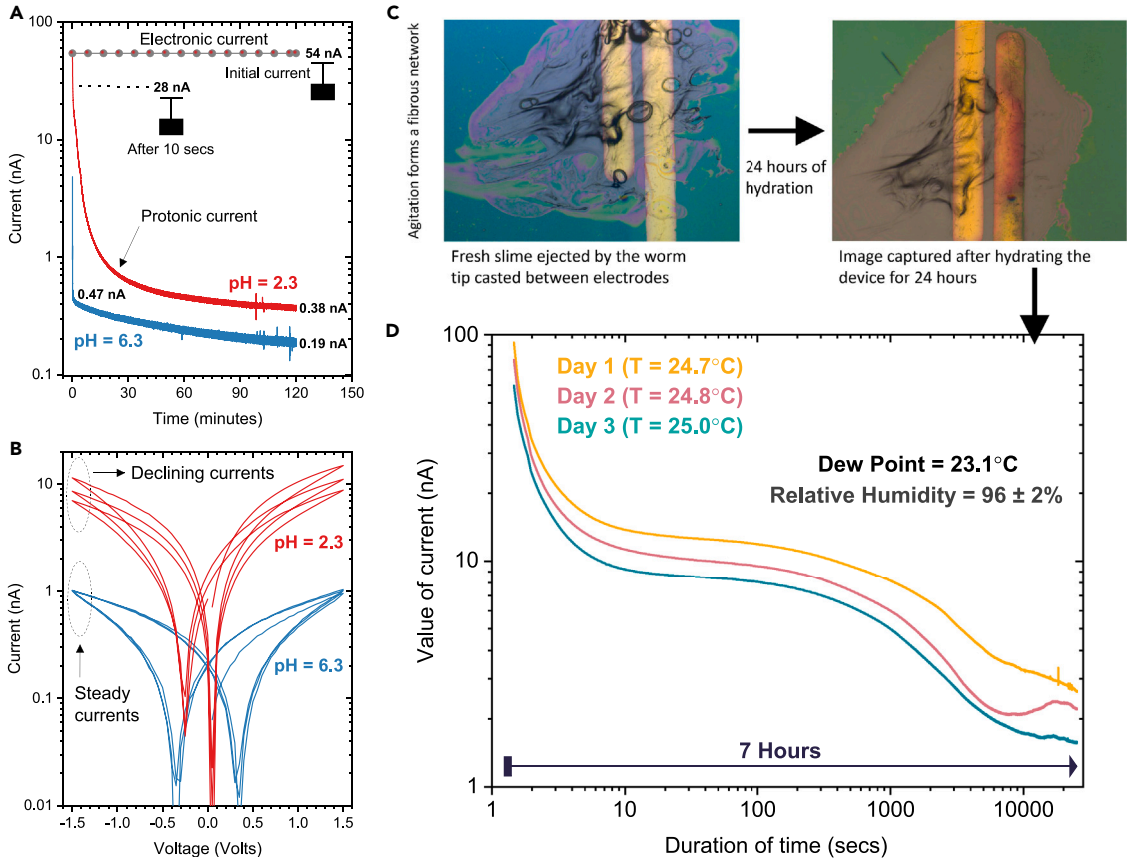

Figure 2. Dependence of electronic and ionic currents on time and protonic currents on pH

(A) Transient decay of current measured continuously over a time period of 2 h at pH levels of 2.3 and 6.3. If this current is purely electronic, it should have remained constant with time as shown by drawing a horizonal dotted line having a value of 54 nA.

(B) I-V characteristics of the device demonstrate that the magnitude of currents has a strong pH dependence.

(C) Optical microscope images of a device fabricated by casting native slime between gold electrodes.

(D) Plot illustrates the decaying trends in current measured over an extended time period of 7 h, repeated three times on consecutive days.

from the bottom through a temperature controlled stage (Figure S2A). Here as well, we observed an initial rise in conductivity that quickly decreased over time and at T ≈ 50°C devices displayed insulting behavior. The hydration dependent variations in the electric current measured for a complete cycle (dry-wet-dry) are shown in Figure S2B.

Dependence of electronic and ionic currents on time and protonic currents on pH

The electrical conductivity induced by water absorption in a proteinaceous substance can be attributed to the motion of either electrons or protons/ions. Theories that are invoked to explain the conductivity of hydrated proteins are disputed.[15] Rosenberg[16,17] showed that a majority of hydrated materials are electronic conductors having an activation energy of ≈3 eV. Alternatively, it has been postulated that hydrated proteins are protonic conductors.[18,19] The dependence of current on degree of hydration is given by the Spivey expression[15] $I_{wet} = I_{dry}\, exp^{\alpha m}$, where I_{dry} and I_{wet} are the current magnitudes in dry and hydrated state, and α is a constant for a particular protein. The nature of charged carriers in solvated biomolecules is typically characterized as a mix of protons and electrons.[20] Rosenberg reasoned that a distinction between electronic and protonic current could be made,[16] on the basis that a protonic current measured for a prolonged time period using ion-blocking electronic conductors will appear as a decaying transient (decline exceeding 90%). While if the conductivity is purely electronic, it will remain relatively constant in time (≈5% decline); and in such hydrated solids water absorption basically increases the dielectric constant, which in turn decreases the activation energy for charge transport as $E_{wet} = E_{dry} - \gamma m$, where E_{wet} and E_{dry} are the activation energy in the wet and dry states, m is the percentage of water absorption, and γ is a T independent constant.[16] Expanding upon Rosenberg's idea, we conducted experiments on aqueous slime at two levels of pH, specifically at pH 2.3 and 6.3 (Figure 2A). In undertaking this experiment, the device was placed in a sealed chamber (RH = 86%) and current was recorded continuously at a constant bias, set below the thermoneutral voltage of water. Over a time period of 2 h, the current dropped >95% from its initial value. Purely electronic currents are not anticipated to decline in this manner as they have a steady-state nature. The I-V curves shown in Figure 2B

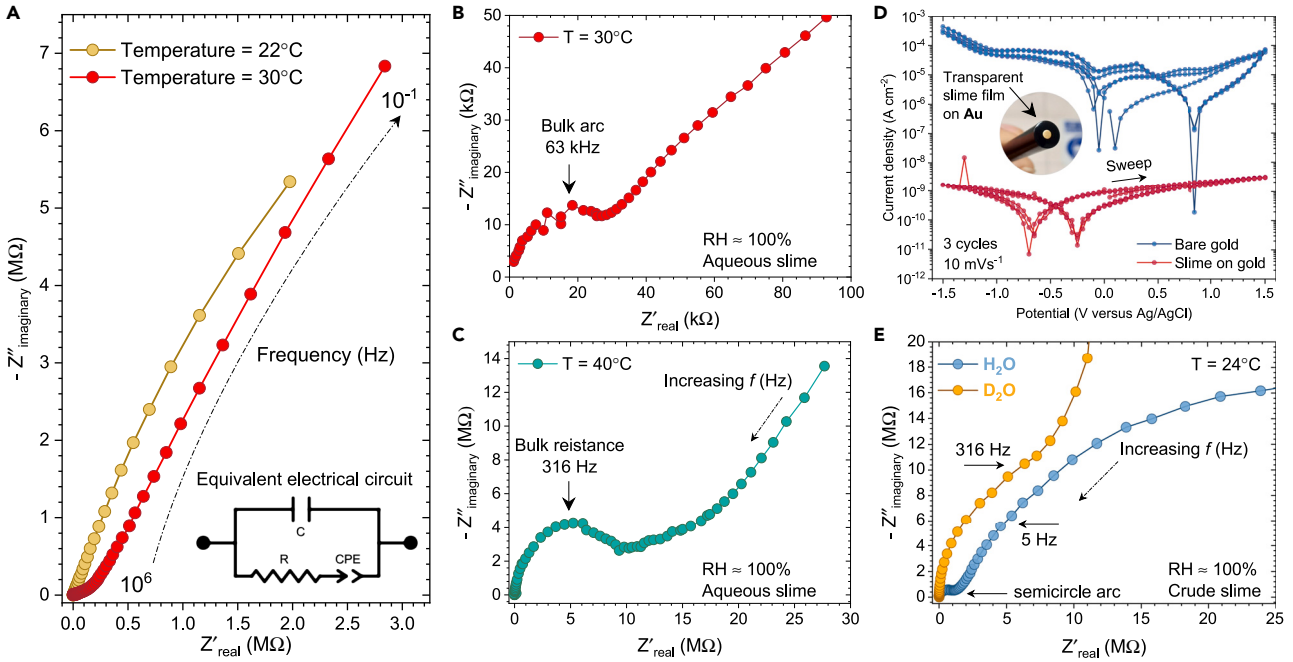

Figure 3. Electrochemical impedance spectroscopy and cyclic voltammetry on slime

(A) Complex plane plots obtained for slime films at 22°C and 30°C. Inset to the figure shows an equivalent electrical circuit which is used for fitting the experimental data.

(B and C) Emergence of a Debye semicircle at 30°C and 40°C in the high frequency region of the Nyquist plots.

(D) Three cycles of CV for bare Au (working electrode) and a thin-film of slime on Au (see inset) measured at a scan rate of 10 mVs^{-1} for the same potentials (-1.5 V to +1.5 V), wherein silver/silver chloride (Ag/AgCl) electrodes act a reference, and platinum as a counter electrode immersed in a buffer solution (water).

(E) Nyquist plots acquired for native slime in presence of H_2O (blue) and D_2O (yellow) vapor.

correspond to the measured data at these pH levels. At acidic pH level of 2.3, the device displayed elevated current levels because of the higher concentration of hydrogen/hydronium ions, and when these I-V curves were recorded successively (3 scans), there was a noticeable decrease in the current value as expected. Such characteristics observed for a set of four devices are shown in Figure S3.

To illustrate that native slime of the velvet worm is a proton conducting material in its hydrated state, we conducted transient measurements on fresh slime ejected by the worm which was immediately casted between electrodes, Figure 2C. Mild agitation involved in the process of casting resulted in the formation of a fibrous network within the film, Figure 2C. While aqueous slime can hydrate instantly, the native slime device was placed in a sealed chamber for a hydration period of 24-h before measurement, Figure 2C. The time duration of experiment was extended up to 7 h, and it was repeated 3 times on consecutive days that displayed a typical decay of electric current between 100 nA and 1 nA, Figure 2D, indicating proton transport in slime. The decay of current is due to the interfacial polarization that occurs because of the accumulation of charge carriers at the partially blocking electrodes, as their rate of arrival at the sample-electrode interface is faster than that of their transfer through diffusion or discharge.[21] It is important to emphasize here that protonic-to-electronic ratio in hydrated conductors may vary with electric field, temperature, and other associated factors.

Temperature and isotope effect in impedance spectroscopy survey

We performed impedance spectroscopy (IS) to examine slime's electrical response to an alternating current (AC) potential. The temperature-dependent Nyquist plots obtained at RH ≈ 100% for an AC potential of 50 mV are shown in Figures 3A–3C. These complex plane diagrams display the real (Z') and imaginary (Z'') part of impedance over a frequency (f) range of 0.1 Hz–1 MHz. Their respective Bode phase angle plots (ϕ *vs* f) and Bode magnitude plots ($|Z|$ *vs* f) are provided in Figure S4. At T ≈ 22°C, only an inclined curve appeared in the complex plane whose impedance magnitude decreased linearly with the increase in frequency, indicating a dominant capacitive behavior up to ≈105 Hz. When the temperature was raised to 30°C, a small Debye semi-circle emerged in the high frequency range (not visible in Figures 3A and 3B) in conjunction with a linear relationship between Z'' with Z' with a slope for f > 40 kHz. The shape of this curve is often considered as a signature of protonic conductivity,[13,22] wherein the extrapolated diameter of the full semi-circle in high frequency range is taken as protonic resistance. Further increase in temperature to 40°C extended the diameter of the semi-circle arc (Z' magnitude) over 0.1 to 10 kHz, indicating an increase in resistance (Figure 3C). At 50°C the low frequency $|Z|$ reaches a value of 0.245 giga-ohms. This observed temperature dependence aligns with DC measurements, Figure 1F.

The shape of the impedance diagrams observed can be understood within the framework of the absolute rate theory.[21] In the dry state or at elevated temperatures, the slime film can be treated as a series of equivalent energy barriers that the mobile carriers must overcome to conduct. When it is exposed to a low level of hydration, independent aqueous microdomains are created as interconnected clusters linked to each other only via a fine narrow channel. As a result, the energy barrier required to overcome two clusters becomes higher than the energy barrier between any adjacent sites in a cluster. Under this condition, charges can accumulate on each side of the narrow channel, resulting in the appearance of capacitive nature. When the slime is exposed to a high degree of hydration, it should be treated as a homogenous medium without any clusters, such that the barrier to the mobile charge within and between the clusters becomes similar in energy. For the resulting increase in film thickness due to swelling, a linear shape is observed in the impedance diagram, while the semicircle appears in the high frequency region only when water content is reduced.[21] We fitted the experimental data with the equivalent electrical circuit (inset to Figure 3A) and simulated the experimentally observed Nyquist plots that represent the real system (Figure S5).

Studying proton conductors commonly involves observing isotope effects in IS. This is achieved by recording the response for H_2O and deuterium oxide (D_2O) hydration,[23] Figure 3E. It is expected that for D_2O[13,24,25] the protonic resistance or the diameter of semicircle would increase because of the dependence of charge transport on mass of the charge carrier. However, isotope effects are often observed unusual[26]—40% change in resistance was observed for reflectin,[13] 5–15% for glycosaminoglycans,[24] 10% for bovine serum albumin,[25] and 0% for melanin.[27] Multiple factors, including the contributions from ions and electrons to the overall current, as well as the mechanism governing charge transport, can influence these measurements. Protons generally exist in their solvated states: for example solvation by water or ammonia leads to the formation of ions such as H_3O^+or NH_4^+. When protons are carried and transported by migration of such ions, it is referred to as the vehicular mechanism. In the Grotthuss mechanism, displacement of H^+ occurs along a network of hydrogen bonds. Here, a lone proton jumps from a donor to an acceptor molecule, typically from H_3O^+ to H_2O or H_2O to OH^-. In this case, isotope effect is not expected to be observed because the relative transfer of mass in a hooping event is negligible. Moreover, to realize such a sensitivity in electrical measurements makes them subtle. We were unable to quantify the % change in resistance, as we cannot fit the Nyquist plot for D_2O, though variation in total impedance for H_2O and D_2O can be seen in Bode plots, Figure S6. The IV curves obtained with D_2O were of the same magnitude as those with H_2O.

Use of metals, metal catalyst, and metal hydride in collecting protonic currents

We examined the electrochemical activity of the slime on gold (Au) electrode using cyclic voltammetry (CV) in a three-electrode configuration, over the same potentials as used in electrical characterization. The voltammograms presented in Figure 3D show that the current density was reduced by five orders of magnitude from 10^{-4} Acm^{-2} for bare Au to 10^{-9} Acm^{-2} for slime on Au (see inset). Unlike Au, the voltammogram for slime did not feature reduction or oxidation peaks for three successive scans (scan rate 10 mVs^{-1}), which suggests that the electronic conductivity associated with oxidation or redox reactions is unlikely in devices fabricated using this metal.

To observe the influence of metal catalysts, we used platinum (Pt) and palladium (Pd) as electronic contacts. The RH dependent I-V curves for these electrodes are presented in Figure 1G, which shows that protonic currents can be collected using these metals. A comparison among them based on the observed current magnitude should be avoided as they are fabricated by drop-casting procedure lacking control over geometric factors such as film thickness and slime-electrode interface area. For a device wherein a protonic current is collected via an electronic conductor, a sustained flow current is possible if a proton-electron exchange occurs continuously at the material-metal interface.[28] It is well-known that this exchange process is efficient if a metal hydride such as PdH_x is used instead of metal contacts. In a separate experiment, we converted Pd films into PdH_x films by exposing them to pure hydrogen gas. This process resulted in a significant decrease in the electronic conductivity of the Pd film by up to 10^9 times—an evidence of the transformation from Pd to $PdH_{0.5}$ (Figure S7).[29] Such a reduction in its conductivity is not ideal when aiming to make a comparison of device performance before and after H_2 exposure, for the geometry of our electrodes having electrode pads 1 mm apart. To reduce the amount of H_2 absorption by Pd, we opted to use for a mixture of argon-hydrogen (5%) and observed that current measured was lower relative to Pd (Figure 1C), probably due to a reduction in the electronic conductivity of PdH_x. The use of PdH_x electrodes may improve charge collection though it might not resolve the charge accumulation issue because the rate of arrival of protonic species at the sample-electrode interface is always faster than their rate of diffusion in PdH_x. Moreover, PdH_x is not a stable hydride: within few hours it transforms back to Pd.

An ionic current measured through an ion-blocking (partially) electronic conductor always appears as transient. It is crucial to underscore that the interpretation of I-V curves in such experiments must be contextualized within the framework of space-charge-limited currents.[28] In our observations, the device showcased the ability to manifest varying current magnitudes, diverse hysteresis, and, notably, negative current magnitudes through simple adjustments: (i) reversing delay voltage polarity and (ii) changing voltage scan rate and also measurement history (Figure S8). As such, simple measurement adjustments can lead to variability in device characteristics that can be wrongly conceived as an experimental error. Direct interpretation of IV curves, especially based solely on their magnitudes, should be avoided. If the observation is genuine and real, it must be replicable in a separate experiment. For instance, we demonstrated a comparable temperature dependency in both I-V and IS, or thermally activated conductivity by altering temperature sources and experimental conditions.

The slime fiber

In the fluidic state, the majority of proteins exist freely in slime whilst 10% of proteins are confined in densely dispersed protein-lipid globular particles.[7,9] A unique characteristic of the slime is its ability to reversibly transform from fluid to solid fibers under ambient conditions.[10] Application of a normal or shear force to the slime results in a structural transition from a viscous solution to fibers, which reduces the density of

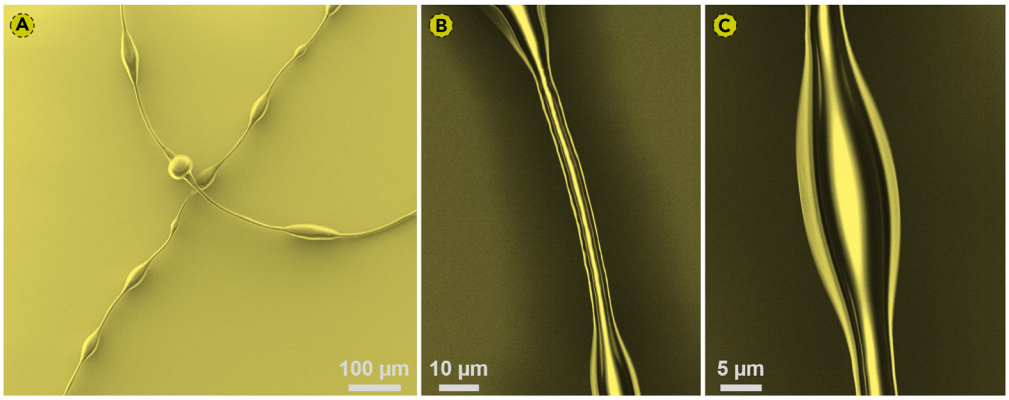

Figure 4. The slime protein fiber

(A) Low-magnification SEM image of a dry slime fiber mechanically drawn from the ejected viscous slime.

(B) A section of the fiber showing its assembly. A protein rich core and a lipid-protein coating with eyelid shaped droplets at both ends.

(C) Zoom-in image of a droplet. The central region of the droplet is charged, clearly indicating this region is non-conductive. The coating of the droplet, which is composed of densely packed co-localized protein-lipid globular particles, can also be seen distinctively.

nanoglobules in the surrounding solution.[11] The resulting fibers are constituted of a proteinaceous core lined with a continuous lipid-protein coating throughout the length of the fibers.[9] The elongation length of the fibers can reach up to few cm with a diameter in some µm. Once drawn, the fibers dry very rapidly but can be redissolved by immersing them for 12 h in water. The dissolution is slow but recyclable, indicating that the protein-lipid interactions in slime are non-covalent in nature, such that they are able to form nanoglobules again in their redissolved state.[10] Scanning electron microscope (SEM) images of a dry slime fiber acquired at a low electron beam acceleration voltage of 5 kV are shown in Figure 4. The structure of the fiber showed that it constituted of equally spaced eyelid-shaped droplets. These droplets are formed on the fiber due to Plateau-Rayleigh instability,[30] which also provides a thin coating to the fiber core.[31] The fibrillization process is an indispensable biological function of slime to seize prey, along with its ability to strongly adhere onto surfaces via the electrostatic interactions.

Electrical conductivity of a slime fiber

We mechanically draw a centimeter-long single fiber (diameter 10.8 µm) from the native slime and connected it across PdH_x electrodes to determine its electrical conductivity, Figures 5A and 5B. The resistivity (ρ) of the fiber dropped three orders in magnitude in hydrated state relative to its dry state (10^6 Ω-m to 10^3 Ω-m), Figure 5C. In order to validate that the measured current in our experiment originates from fiber hydration and not from any water condensation between the electrodes, we first measured the response of bare electrodes under the same measurement conditions, Figure S9. A change in electric current as a function of RH was measured that slowly increased with time for fiber before it attained its maximum value, Figure 5D. When dry fibers were hydrated in a saturated chamber for a prolonged period, their morphology was transformed permanently (Figure S10). The eyelid-shaped droplet transformed into a spherical shape (inset to Figures 5C and S11). The dark-field and bright-field optical microscopy images presented in Figures 5G and 5H acquired over a section of fiber illustrate the hydration-induced hierarchical assembly of it building blocks. The conductivity of the fiber was determined using the equation $\sigma = GL/A$, where G is the conductance ($1/R = 1.06 \times 10^{-6}\ \Omega^{-1} \pm 9.58\%$), Figure S12), A is the cross-sectional area of the hydrated fiber ($\approx 265\ \mu m^2$) and L is channel length ≈ 100 µm, yielding $\sigma_{H^+} \approx 4$ mS cm^{-1}. This value is higher than that of Sharks Jelly which is known to have the highest conductivity among natural biomaterials.[12,32] Both slime and jelly are stored within the bodies of animals in a fully hydrated state. Note that absolute proton conductivity cannot be determined precisely by such experimental protocols.[21] Conductivity calculated using I-V dataset was found one order lower in magnitude, while average conductivity calculated using EIS data was $\approx 2.42 \pm 1.18$ mS cm^{-1} measured for three devices (Figure S13). Regardless, a change in the conductivity forms the basis for device development, not necessarily requiring high conductivity—which only offers faster operations and, in some cases, lower power losses. A contrast among biomaterials sourced from various origins and their reported conductivity is presented in Table S1. Further, to supplement our measurements, we evaluated the I-V and transient response of large-area devices fabricated using long fibers, Figures S14 and S15.

Origin of hydrated protonic conductivity

Our results unambiguously demonstrate protonic conductivity in slime films and fibers, raising the question about the origin of proton conductivity and whether it has a physiological role for the velvet worm. The slime proteins are mostly intrinsically disordered, highly charged, and primarily comprises of multiple high molecular weight proteins (MW) > 250 kDa as seen in the SDS-PAGE characterization shown in Figure 5E (lane 2). We have recently obtained the full-length primary sequence of amino acids in slim and revealed that these high MW proteins contain cysteine (Cys) residues that regulate the formation of multi-proteins via disulphide bonding.[33] The Fourier transform infrared (FTIR) spectrum of the dry slime presented in Figure 5F features all protein amide bands. The hydrated slime spectrum confirmed the strong absorption of water molecules by the slime, with H_2O peak at 3,300 cm^{-1} and 2,100 cm^{-1} that dominates over the protein backbone vibrations (Figure 5F).

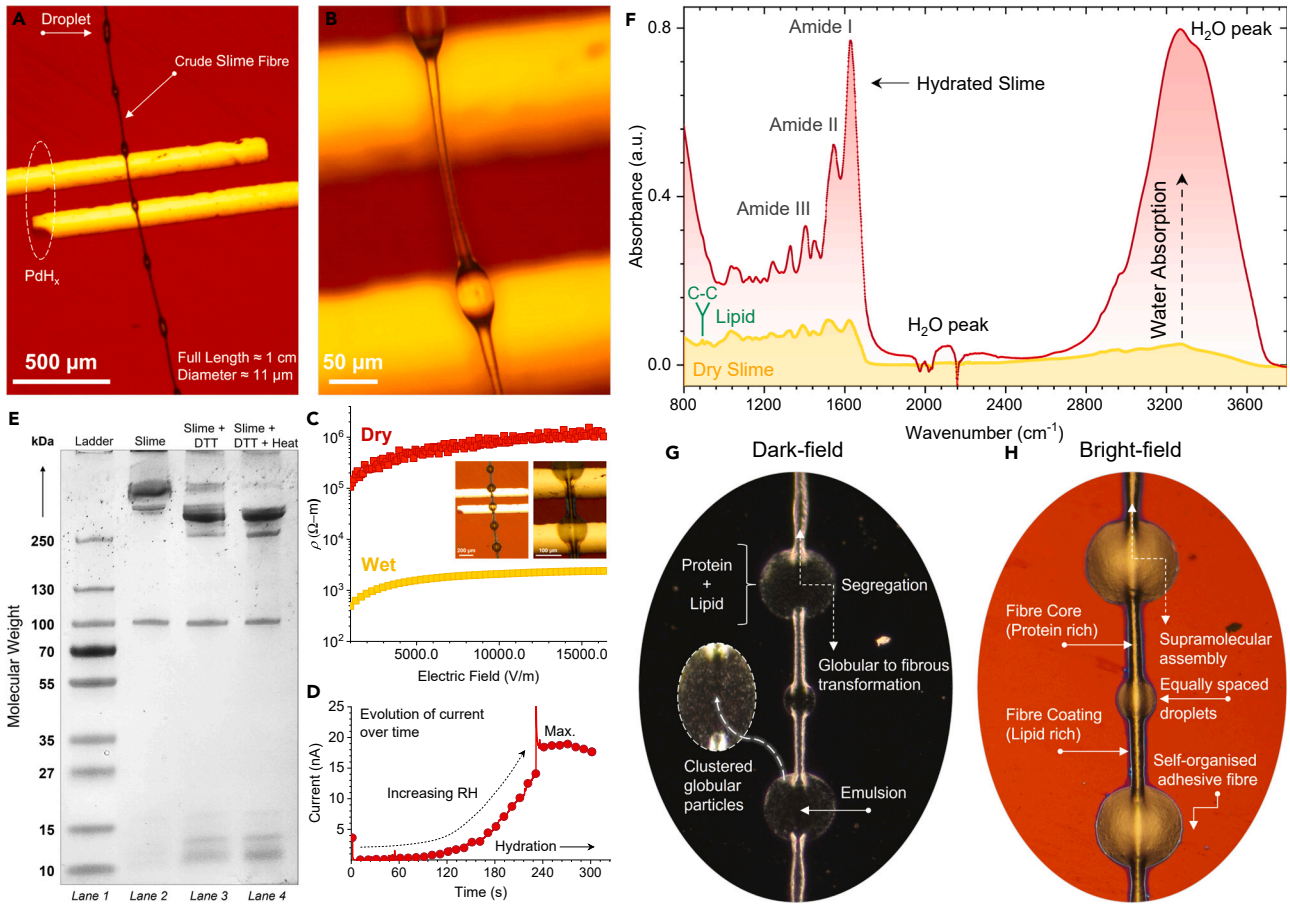

Figure 5. Dry and hydrated slime

(A) Optical image of a microfibre device, fabricated by bridging a dry fiber across PdHx contacts.

(B) Zoom-in image of the fiber, showing that the fiber comprises of a core, a coating, and also equally spaced droplets.

(C) Change in the resistivity of the fiber device under dry and hydrated conditions. Inset to the figure shows expansion of fiber after hydration (see Figure S11).

(D) Evolution of device current over time with the increase in water absorption until it reaches a maximum value (5 min).

(E) SDS-PAGE characterization of aqueous slime. Lane 1 is the protein ladder as MW reference. Lane 2 is the untreated slime comprising of multiple high MW proteins (>250 kDa) in a complex. Lane 3 shows the slime treated with dithiothreitol (DTT) that cleaves the disulfide bonds within slime proteins. The proteins in the top-most band are separated from the complex, along with some low MW proteins. Lane 4 shows the slime heated after treatment with DTT, which further breaks down intermolecular interactions of the high MW complex at the top of the gel.

(F) FTIR spectrum of dry and hydrated slime.

(G and H) Dark-field and bright-field microscopy images of a hydrated slime fiber. Once hydrated, the fiber strongly adheres on to the surface, and it cannot be removed even with a continuous flush of water.

The absorption of water led to an increase in film thickness (aqueous slime) up to ≈100 nm relative to dry film. Consequently, the film reflects light at different wavelengths due to thin-film interference effect, producing an intense coloration. As we show in Figure S16, the optical reflectance of such films can be blue and red shift across the whole visible spectrum.

Proton conductivity principally originates due to hygroscopic properties of composition of its dry state constituents. The amino acid composition of the slime proteins of the velvet worm species used in this study is provided in Table S3. Slime has a high glycine content (≈37%), along with glutamic acid (≈11%) and aspartic acid (≈8%). These three amino acids are known to have high proton conducting properties.[34–36] Slime proteins are also phosphorylated,[6,10,33] and such residues may contribute protons, as reported for supercharged proteins enriched in acidic residues.[37] In fact, negatively charged groups are deliberately added in commercially available polymers to impart proton conductivity, such as phosphorylated side chains in BSA proteins[38] and graphene oxide.[39] Slime proteins are glycosylated,[5,24,40] which improves their hydrophilicity and consequently results in efficient diffusion of water molecules. Recently, glycoproteins have been framed as a starting material for developing biocompatible proton conductors.[41] Slime proteins contain repeat domains 20 to 30 amino acids long enriched in positively charged residues that organize as lysine (Lys) and arginine (Arg) dipeptides (RR, KK, and RK motifs). These dipeptide motifs are protonated (at physiological pH conditions) and may be able to provide proton donating sites. Molecular dynamic simulations as well as

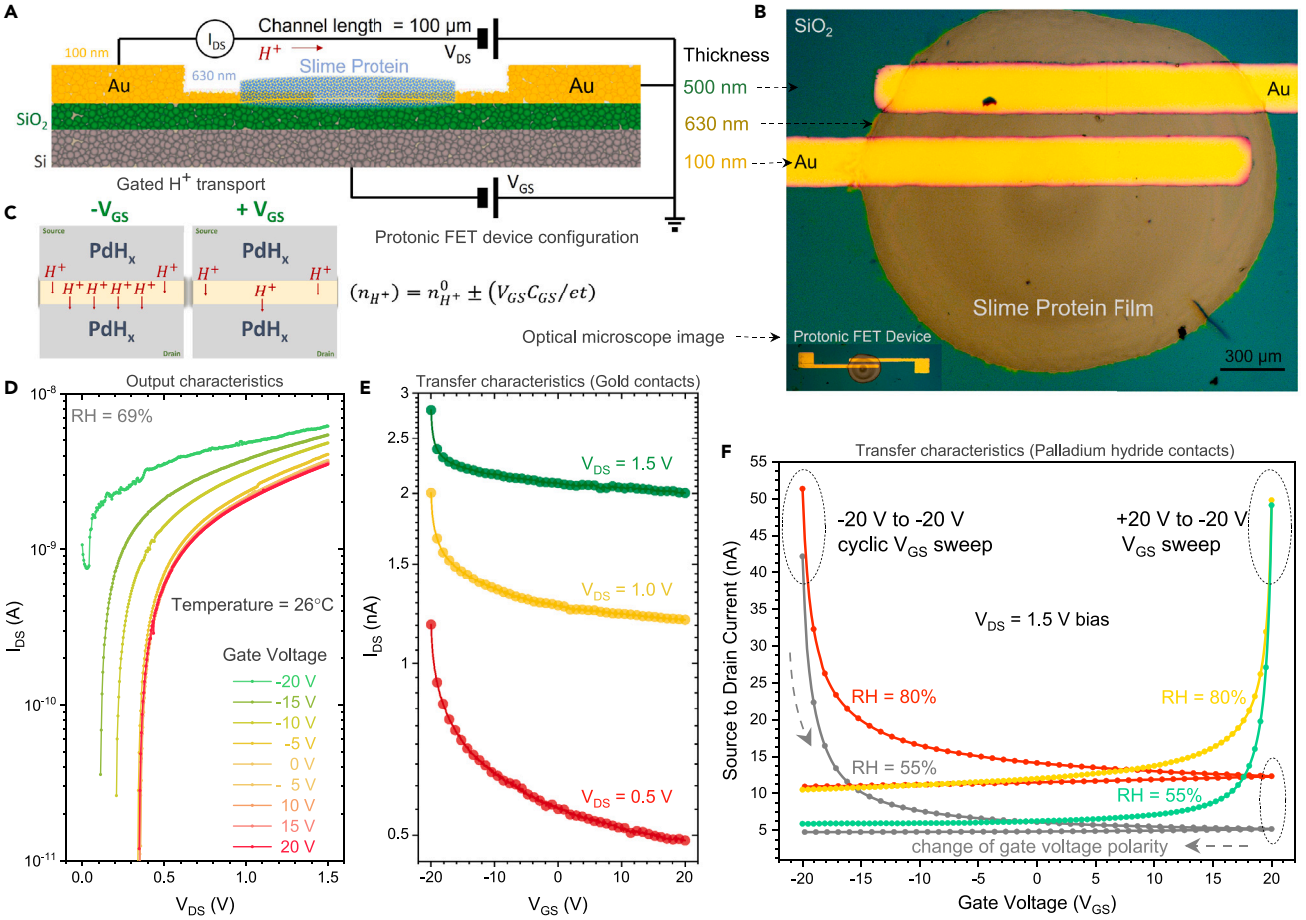

Figure 6. Field-effect transistor (FET) devices

(A) Schematic diagram depicting a three-terminal FET device configuration with Au electrodes and SiO2 gate dielectric. In the same configuration, we fabricated FETs with PdHx electrodes and HfO2 gate dielectric.

(B) Optical image of the actual FET device.

(C) Schematic illustration showing an expected change in proton charge carrier density due to the effect of positive or negative electrostatic gating.[13,43]

(D and E) Output and transfer characteristics of the FET device, respectively.

(F) Transfer characteristics of the FET device with PdH_x electrodes. The transfer curves are presented for RH of 55% (gray curve) and 80% (red curve) acquired by negative-to-positive and then back to negative gate voltage (cyclic gate voltage sweep), green and yellow curves are obtained by a positive-to-negative voltage sweep.

experiments results on Lys- and Arg-rich peptides have shown that the presence of such side chains significantly enhances proton conductivity, with Lys displaying an order magnitude higher conductivity than Arg.[42] We posit that these intrinsic attributes of slime constituents may facilitate a charge transport in their hydrated state. Proton conductivity discovered in electro-sensory organs of sharks and skates[32] has been suggested to play a central role in detecting extremely weak electric fields produced by the prey. Velvet worms may exploit a similar mechanism, but this remains speculative.

Hygroscopic field-effect transistors

We utilized slime to fabricate field-effect transistor (FET) on complementary Si/SiO_2 substrate. Figure 6A illustrates the FET device configuration schematically, while Figure 6B displays an optical microscope image of the device featuring Au electrodes. The surface roughness profile (max. variation of ±20 nm) of the film acquired after its repeated hydration is shown in Figure S17. The output characteristics of the FET are presented as a set of currents acquired at different gate voltages (V_{GS}) from −20 V to +20 V (Figure 6D), and its transfer characteristics are shown in Figure 6E. Both characteristics of the device as a function of RH (44%, 66%, 77%, and 88%) is shown in Figure S18. High RH levels can lead to short circuiting through gate electrode. To circumvent this issue, we isolated the device as well as the substrate using Poly (methyl methacrylate) that enabled very low leakage currents, Figure S19. Throughout this study, we have demonstrated that protonic currents manifest as transients rather than steady-state currents when measured using partially blocking electrodes. This nature of electric current can

overshadow a true electrostatic gating effect. The systematic decline observed in the characteristics of FETs may simply be a protonic transient. The working principle of such FETs with PdH_x electrodes is described in the early reports.[13,43] When a negative gate voltage is applied, proportional positive charges are induced in the channel as the conducting silicon substrate and electrodes form a capacitor with an oxide dielectric between them. To create additional positive charges, protons are injected into the channel from electrodes, thereby increasing the concentration of charges (n_{H^+}), and hence the conductivity (σ_{H^+}) = $e.\mu_{H^+}.n_{H^+}$, where e is the elementary charge and μ_{H^+} is the mobility of the protonic species. Application of positive gate voltages depletes the protonic charge density, as shown schematically in inset to Figure 6C. Using the previously established protocol,[13,43] we estimated μ_{H^+} from the linear fit to the slope of conductivity $\left(\pm\frac{\partial\sigma}{\partial V_{GS}}\right)$ versus gate voltages plot using $\mu_{H^+} = \pm\frac{\partial\sigma}{\partial V_{GS}}\frac{t}{C_{GS}}$. We obtained a protonic mobility (μ_{H^+}) of 3.4×10^{-4} $cm^2 V^{-1}s^{-1}$ and a protonic charge carrier density ($n^0_{H^+}$) of *ca.* 3.86×10^{17} cm^{-3} at zero gate bias. The electrostatic gating is associated with the change in total charge carrier density that follows: $(n_{H^+}) = n^0_{H^+} \pm (V_{GS}C_{GS}/et)$, where V_{GS} is the gate voltage, C_{GS} is the gate capacitance, and t is the film thickness. Errors are linked to these estimated values due to the inability to precisely measure the t in the channel.

We also fabricated FET with PdH_x contact whose transfer characteristics are shown in Figure 6F. This figure has four transfer curves, which were all acquired for a source to drain voltage of 1.5 V. Yellow (RH = 80%) and green (RH = 55%) curves were recorded by sweeping the gate voltage from +20 V and stopping at −20 V. The red (RH = 80%) and gray (RH = 55%) curves were recorded by sweeping the gate voltage from −20 V to +20 V then back to −20 V, in one single scan. The current displayed transient behavior within the range of −20 V to +20 V, but upon an abrupt reversal of gate polarity, the current stabilized into a steady state. We conclude that expected variation in current magnitude (schematic presented in Figure 6C) in response to the change in polarity of the gate voltage was not observed in such measurements at the scan rate and delay time used in the measurements. It is however interesting to note that upon sudden reversal of gate voltage polarity (sweep direction), the decline in current was halted and became steady. Since the magnitude and the polarity of source to drain voltage are constant, and only the direction of gate voltage sweep was altered—this effect should be related to electrostatic gating or otherwise accumulation of charges at one electrode interface. The stead-state current has an electronic nature, and it is unaffected by gate bias. We believe an effective modulation of electrical currents via gating is possible if the use of gate potential can increase or decrease the efficiency of the proton-electron exchange process at the sample-electrode interface, which is localized only in the vicinity of source and drain electrodes, for example by controlling the diffusion of protonic charges into metal hydrides at the drain. Table S2 compares the device metrics of all FETs based on proton conductors reported since their initial demonstration.

Conclusion

Proton conductivity is utilized in operations of electrochemical cells and bioenergetic of living cells. Research efforts have increased to expand the usage for proton conductivity, in particular to fabricate protonic devices. In parallel, there is strong interest in sustainable alternative materials for the development of small-scale proton-exchange membranes to be employed in green energy technologies. Biopolymers are the ideal choice for such applications as they are solution processable, biodegradable, and compatible with living systems. However, design guidelines for proton conductors have been lacking to chemically synthesize high-performance biopolymers. In contrast to other materials, slime has the capability to spontaneously form high aspect ratio flexible fibers that not only exhibit high conductivity but also mechanical strength, electrical durability, flexibility, and recyclability. The biochemical composition of the slime can serve as molecular-level design guidelines such that it can be mimicked synthetically. From this perspective, we anticipate that our findings on slime of the velvet worm can serve as a valuable reference for the design and development of proton conducting materials.

Limitations of the study

A limitation of the study is related to the small amount of slime that can be obtained from a single animal, which required to use slime secreted from different individual for comprehensive characterization of the electrical transport properties. This limitation can affect reproducibility of the measured electric properties. In addition, it should be emphasized that proton-conducting properties are always assessed using indirect electrical measurements methods since protonic current cannot be directly measured.

STAR★METHODS

Detailed methods are provided in the online version of this paper and include the following:

- KEY RESOURCES TABLE
- RESOURCE AVAILABILITY
  - Lead contact
  - Materials availability
  - Data and code availability
- EXPERIMENTAL MODEL AND STUDY PARTICIPANT DETAILS
- METHOD DETAILS
  - Slime sample collection
  - Coomassie blue staining of aqueous slime
  - Fabrication of devices

- Electrical characterization of devices
- Optical and physical characterization of films

- QUANTIFICATION AND STATISTICAL ANALYSIS

SUPPLEMENTAL INFORMATION

Supplemental information can be found online at https://doi.org/10.1016/j.isci.2024.110216.

ACKNOWLEDGMENTS

This research was supported by the Singapore Energy Research Center (SgEC). The authors thank Prof. Nripan Matthews and Dr. Si En Timothy Ng for the use of electron-beam deposition system, and Prof. Cesare Soci for the use of source measurement unit for the characterization of electrical devices.

AUTHOR CONTRIBUTIONS

A.M. conceived the idea to study slime of the velvet worm. R.S. planned and executed the experiments with the co-authors; R.S. (electrical measurements), R.S. and B.S. (sample preparation and material characterization), R.S. and M.K. (FET device fabrication and characterization), R.S. and J.J.L. (optical measurements), R.S. and Q.M.P. (SEM imaging), R.S. analyzed the data and wrote the manuscript with A.M. and inputs from all co-authors. A.M. supervised the overall project.

DECLARATION OF INTERESTS

The authors declare no competing interests.

Received: April 29, 2024
Revised: May 16, 2024
Accepted: June 5, 2024
Published: June 8, 2024

REFERENCES

1. Blaxter, M., and Sunnucks, P. (2011). Velvet worms. Curr. Biol. *21*, R238–R240. https://doi.org/10.1016/j.cub.2011.02.017.
2. Beckmann, H., Hering, L., Henze, M.J., Kelber, A., Stevenson, P.A., and Mayer, G. (2015). Spectral sensitivity in Onychophora (velvet worms) revealed by electroretinograms, phototactic behaviour and opsin gene expression. J. Exp. Biol. *218*, 915–922. https://doi.org/10.1242/jeb.116780.
3. Oliveira, I.d.S., Franke, F.A., Hering, L., Schaffer, S., Rowell, D.M., Weck-Heimann, A., Monge-Nájera, J., Morera-Brenes, B., and Mayer, G. (2012). Unexplored Character Diversity in Onychophora (Velvet Worms): A Comparative Study of Three Peripatid Species. PLoS One *7*, e51220. https://doi.org/10.1371/journal.pone.0051220.
4. Concha, A., Mellado, P., Morera-Brenes, B., Sampaio Costa, C., Mahadevan, L., and Monge-Nájera, J. (2015). Oscillation of the velvet worm slime jet by passive hydrodynamic instability. Nat. Commun. *6*, 6292. https://doi.org/10.1038/ncomms7292.
5. Benkendorff, K., Beardmore, K., Gooley, A.A., Packer, N.H., and Tait, N.N. (1999). Characterisation of the slime gland secretion from the peripatus, Euperipatoides kanangrensis (Onychophora: Peripatopsidae). Comp. Biochem. Physiol. B Biochem. Mol. Biol. *124*, 457–465. https://doi.org/10.1016/S0305-0491(99)00145-5.
6. Haritos, V.S., Niranjane, A., Weisman, S., Trueman, H.E., Sriskantha, A., and Sutherland, T.D. (2010). Harnessing disorder: onychophorans use highly unstructured proteins, not silks, for prey capture. Proc. Biol. Sci. *277*, 3255–3263. https://doi.org/10.1098/rspb.2010.0604.
7. Baer, A., Hoffmann, I., Mahmoudi, N., Poulhazan, A., Harrington, M.J., Mayer, G., Schmidt, S., and Schneck, E. (2023). The Internal Structure of the Velvet Worm Projectile Slime: A Small-Angle Scattering Study. Small *19*, 2300516. https://doi.org/10.1002/smll.202300516.
8. Rühs, P.A., Bergfreund, J., Bertsch, P., Gstöhl, S.J., and Fischer, P. (2021). Complex fluids in animal survival strategies. Soft Matter *17*, 3022–3036. https://doi.org/10.1039/D1SM00142F.
9. Baer, A., Schmidt, S., Haensch, S., Eder, M., Mayer, G., and Harrington, M.J. (2017). Mechanoresponsive lipid-protein nanoglobules facilitate reversible fibre formation in velvet worm slime. Nat. Commun. *8*, 974. https://doi.org/10.1038/s41467-017-01142-x.
10. Baer, A., Hänsch, S., Mayer, G., Harrington, M.J., and Schmidt, S. (2018). Reversible Supramolecular Assembly of Velvet Worm Adhesive Fibers via Electrostatic Interactions of Charged Phosphoproteins. Biomacromolecules *19*, 4034–4043. https://doi.org/10.1021/acs.biomac.8b01017.
11. Baer, A., Horbelt, N., Nijemeisland, M., Garcia, S.J., Fratzl, P., Schmidt, S., Mayer, G., and Harrington, M.J. (2019). Shear-Induced β-Crystallite Unfolding in Condensed Phase Nanodroplets Promotes Fiber Formation in a Biological Adhesive. ACS Nano *13*, 4992–5001. https://doi.org/10.1021/acsnano.9b00857.
12. Jia, M., Kim, J., Nguyen, T., Duong, T., and Rolandi, M. (2021). Natural biopolymers as proton conductors in bioelectronics. Biopolymers *112*, e23433. https://doi.org/10.1002/bip.23433.
13. Ordinario, D.D., Phan, L., Walkup, W.G., 4th, Jocson, J.-M., Karshalev, E., Hüsken, N., and Gorodetsky, A.A. (2014). Bulk protonic conductivity in a cephalopod structural protein. Nat. Chem. *6*, 596–602. https://doi.org/10.1038/nchem.1960.
14. Rieke, P.C., and Vanderborgh, N.E. (1987). Temperature dependence of water content and proton conductivity in polyperfluorosulfonic acid membranes. J. Membr. Sci. *32*, 313–328. https://doi.org/10.1016/S0376-7388(00)85014-0.
15. Turnbull, J.H., Weiss, J., Butler, J.A.V., Szent-Györgyi, A., Chance, B., Baughan, E.C., Paoloni, L., Eley, D., Mason, R., Longuet-Higgins, H.C., et al. (1959). General discussion. Discuss. Faraday Soc. *27*, 232–272. https://doi.org/10.1039/DF9592700232.
16. Rosenberg, B. (1962). Electrical Conductivity of Proteins. Nature *193*, 364–365. https://doi.org/10.1038/193364a0.
17. Rosenberg, B. (1962). Electrical Conductivity of Proteins. II. Semiconduction in Crystalline Bovine Hemoglobin. J. Chem. Phys. *36*, 816–823. https://doi.org/10.1063/1.1732615.
18. Tredgold, R.H., Sproule, R.C., and McCanny, J. (1976). Proton conduction in protein films. J. Chem. Soc., Faraday Trans. 1 *72*, 509–512. https://doi.org/10.1039/F19767200509.
19. Algie, J.E., Downes, J.G., and Mackay, B.H. (1960). Electrical Conduction in Keratin. Textil. Res. J. *30*, 432–434. https://doi.org/10.1177/004051756003000603.

20. Powell, M.R., and Rosenberg, B. (1970). The nature of the charge carriers in solvated biomacromolecules. J. Bioenerg. *1*, 493–509. https://doi.org/10.1007/BF01517187.
21. Colomban, P. (2008). Proton Conductors: Solids, Membranes and Gels - Materials and Devices (Cambridge University Press).
22. Fop, S., McCombie, K.S., Wildman, E.J., Skakle, J.M.S., Irvine, J.T.S., Connor, P.A., Savaniu, C., Ritter, C., and McLaughlin, A.C. (2020). High oxide ion and proton conductivity in a disordered hexagonal perovskite. Nat. Mater. *19*, 752–757. https://doi.org/10.1038/s41563-020-0629-4.
23. Rienecker, S.B., Mostert, A.B., Schenk, G., Hanson, G.R., and Meredith, P. (2015). Heavy Water as a Probe of the Free Radical Nature and Electrical Conductivity of Melanin. J. Phys. Chem. B *119*, 14994–15000. https://doi.org/10.1021/acs.jpcb.5b08970.
24. Selberg, J., Jia, M., and Rolandi, M. (2019). Proton conductivity of glycosaminoglycans. PLoS One *14*, e0202713. https://doi.org/10.1371/journal.pone.0202713.
25. Amdursky, N., Wang, X., Meredith, P., Bradley, D.D.C., and Stevens, M.M. (2016). Long-Range Proton Conduction across Free-Standing Serum Albumin Mats. Adv. Mater. *28*, 2692–2698. https://doi.org/10.1002/adma.201505337.
26. Mostert, A.B. (2022). The importance of water content on the conductivity of biomaterials and bioelectronic devices. J. Mater. Chem. B *10*, 7108–7121. https://doi.org/10.1039/D2TB00593J.
27. Sheliakina, M., Mostert, A.B., and Meredith, P. (2018). Decoupling Ionic and Electronic Currents in Melanin. Adv. Funct. Mater. *28*, 1805514. https://doi.org/10.1002/adfm.201805514.
28. Glasser, L. (1975). Proton conduction and injection in solids. Chem. Rev. *75*, 21–65. https://doi.org/10.1021/cr60293a002.
29. Earnshaw, A., and Greenwood, N.N. (1997). Chemistry of the Elements, 2nd Edition.
30. Haefner, S., Benzaquen, M., Bäumchen, O., Salez, T., Peters, R., McGraw, J.D., Jacobs, K., Raphaël, E., and Dalnoki-Veress, K. (2015). Influence of slip on the Plateau–Rayleigh instability on a fibre. Nat. Commun. *6*, 7409. https://doi.org/10.1038/ncomms8409.
31. Quéré, D. (1999). FLUID COATING ON A FIBER. Annu. Rev. Fluid Mech. *31*, 347–384. https://doi.org/10.1146/annurev.fluid.31.1.347.
32. Josberger, E.E., Hassanzadeh, P., Deng, Y., Sohn, J., Rego, M.J., Amemiya, C.T., and Rolandi, M. (2016). Proton conductivity in ampullae of Lorenzini jelly. Sci. Adv. *2*, e1600112. https://doi.org/10.1126/sciadv.1600112.
33. Lu, Y., Sharma, B., Soon, W.L., Shi, X., Zhao, T., Lim, Y.T., Sobota, R.M., Hoon, S., Pilloni, G., Usadi, A., et al. (2022). Complete Sequences of the Velvet Worm Slime Proteins Reveal that Slime Formation is Enabled by Disulfide Bonds and Intrinsically Disordered Regions. Adv. Sci. *9*, 2201444. https://doi.org/10.1002/advs.202201444.
34. Zheng, Y., Zhou, Z., Jiao, M., Wang, L., Zhang, J., Wu, W., and Wang, J. (2023). Lamellar membrane with orderly aligned glycine molecules for efficient proton conduction. J. Membr. Sci. *672*, 121433. https://doi.org/10.1016/j.memsci.2023.121433.
35. Wang, H., Zhuang, X., Wang, X., Li, C., Li, Z., Kang, W., Yin, Y., Guiver, M.D., and Cheng, B. (2019). Proton-Conducting Poly-γ-glutamic Acid Nanofiber Embedded Sulfonated Poly(ether sulfone) for Proton Exchange Membranes. ACS Appl. Mater. Interfaces *11*, 21865–21873. https://doi.org/10.1021/acsami.9b01200.
36. Nagao, Y., and Matsui, J. (2019). Anisotropic Proton Conductivity of Poly(aspartic acid) Thin Films. Mater. Today: Proc. *17*, 953–958. https://doi.org/10.1016/j.matpr.2019.06.448.
37. Ma, C., Dong, J., Viviani, M., Tulini, I., Pontillo, N., Maity, S., Zhou, Y., Roos, W.H., Liu, K., Herrmann, A., and Portale, G. (2020). De novo rational design of a freestanding, supercharged polypeptide, proton-conducting membrane. Sci. Adv. *6*, eabc0810. https://doi.org/10.1126/sciadv.abc0810.
38. Nandi, R., Agam, Y., and Amdursky, N. (2021). A Protein-Based Free-Standing Proton-Conducting Transparent Elastomer for Large-Scale Sensing Applications. Adv. Mater. *33*, 2101208. https://doi.org/10.1002/adma.202101208.
39. Bai, H., Li, Y., Zhang, H., Chen, H., Wu, W., Wang, J., and Liu, J. (2015). Anhydrous proton exchange membranes comprising of chitosan and phosphorylated graphene oxide for elevated temperature fuel cells. J. Membr. Sci. *495*, 48–60. https://doi.org/10.1016/j.memsci.2015.08.012.
40. Röper, H. (1977). Analytische Untersuchungen des Wehrsekretes von Peripatopsis moseleyi (Onychophora)/ Analytical Investigations of the Defensive Secretion from Peripatopsis moseleyi (Onychophora). Z. Naturforsch. C Biosci. *32*, 57–b. https://doi.org/10.1515/znc-1977-1-208.
41. Yang, Z., Sarkar, A.K., and Amdursky, N. (2023). Glycoproteins as a Platform for Making Proton-Conductive Free-Standing Biopolymers. Biomacromolecules *24*, 1111–1120. https://doi.org/10.1021/acs.biomac.2c01007.
42. Roy, S., Zheng, L., Silberbush, O., Engel, M., Atsmon-Raz, Y., Miller, Y., Migliore, A., Beratan, D.N., and Ashkenasy, N. (2021). Mechanism of Side Chain-Controlled Proton Conductivity in Bioinspired Peptidic Nanostructures. J. Phys. Chem. B *125*, 12741–12752. https://doi.org/10.1021/acs.jpcb.1c08857.
43. Zhong, C., Deng, Y., Roudsari, A.F., Kapetanovic, A., Anantram, M.P., and Rolandi, M. (2011). A polysaccharide bioprotonic field-effect transistor. Nat. Commun. *2*, 476. https://doi.org/10.1038/ncomms1489.

STAR★METHODS

KEY RESOURCES TABLE

REAGENT or RESOURCE	SOURCE	IDENTIFIER
Biological samples		
Slime	Velvet worm	*Eoperipatus sp*
Others		
Metal-based InterDigitated Electrodes (IDEs)	MicruX Technologies	ED-IDE1-Au
Software and alogrithms		
EIS Spectrum Analyser	Aliaksandr Bandarenka and Genady Ragoisha	http://www.abc.chemistry.bsu.by/vi/analyser/
ImageJ	National Institutes of Health	https://imagej.net/ij/download.html

RESOURCE AVAILABILITY

Lead contact

Further information, request for resources and data should be directed to and will be fulfilled by the lead contact, Ali Miserez (ali.miserez@ntu.edu.sg).

Materials availability

This study did not generate any new materials.

Data and code availability

All the raw data as well as the additional information necessary for reanalysing the data presented in this paper, will be provided by the lead contact upon request.

EXPERIMENTAL MODEL AND STUDY PARTICIPANT DETAILS

In this work, slime from the velvet worm specimens of *Eoperipatus sp.* is studied. Specimens were collected in the local secondary forest in Singapore near the Island's coast (Permit No NP/RP19-037 from the National Parks Board, Singapore) and were maintained in plastic boxes with perforated lids. The worms were kept in a thick layer of moist sphagnum moss at cool temperatures (20–24°C), which was cleaned and replenished regularly. The worms were fed with crickets each week. The frequency of slime collection was restricted (twice a month) to avoid unnatural death of worms.

METHOD DETAILS

Slime sample collection

To collect the native slime, velvet worms were gently agitated by sweeping their body with a paintbrush. The squirted slime was left under ambient conditions to dry. Solid dry flakes were then collected and re-dissolved in water over time (10-12 hours) to prepare aqueous solution of slime. The concentration of aqueous slime solution used in this study varies from 0.6-2.3 mg-mL^{-1}. Slime fibres used in this were mechanically drawn from the freshly ejected slime.

Coomassie blue staining of aqueous slime

8 μL of mg mL^{-1}slime samples, untreated or treated with 1,4-Dithiothreitol (DTT), were loaded in each well of Mini-PROTEAN® TGX™ Precast Gels (Bio-Rad) for the polyacrylamide gel electrophoresis (PAGE). Each sample was mixed with 2 μL of 4x Laemmli protein sample buffer. PageRuler™ plus prestained protein ladder (ThermoFisher) was loaded to Lane 1 as the molecular weight reference. Slime re-dissolved in water was added to Lane 2, slime mixed with 10 mM DTT was added to Lane 3, and slime mixed with 10 mM DTT and heated for 3 min at 95°C was added to Lane 4. Electrophoresis was carried out in a Mini-PROTEAN Tetra Cell at 120 V constant voltage till the dye front reached the bottom of the gel. After electrophoresis, the gel was removed from the cast and rinsed in Milli-Q water thrice for 10 min each to remove residual sodium dodecyl sulfate (SDS). The gel was covered with Bio-Safe™ Coomassie Stain and left for gentle shaking for 1 h. After staining, the gel was rinsed in Milli-Q water for 1 h and the proteins were imaged.

Fabrication of devices

Slime based two-terminal electrical devices were fabricated on glass/plastic/Si substrates that featured interdigitated Au/Pt/Pd and PdH_x electrodes. For EIS measurements, standard electrodes (interdigitated spacing = 10 μm) were bought from MicruX Technologies that

were specially designed in a circular cell (diameter = 3.5 mm) for small volume liquid samples such that the drop shape is well-adapted to the electrode cell. Field-effect transistor devices were fabricated by depositing metal electrodes on top of silicon dioxide (500 nm) and hafnium dioxide (50 nm) coated on a silicon substrate. Substrates were first cleaned using acetone, isopropyl alcohol and deionized water using ultrasonication for 10 mins and dried using nitrogen gas. Metal electrodes were then deposited using electron-beam evaporation. An adhesion layer of chromium (10 nm) was deposited first followed by deposition of 100 nm Au/Pt/Pd on top of SiO_2 through a shadow mask. PdH_x electrodes were fabricated by exposing the Pd electrodes to a pure hydrogen gas and argon-hydrogen for 10 minutes in a closed chamber. The device has a channel length of 100 μm and width of 1 mm. Aqueous solution of the slime was then drop casted (≈ 1-5 μL) on to the electrodes and left to dry for 30 mins.

Electrical characterization of devices

The characterization of devices (EIS, I-V, and FET) was conducted in a custom-built dry box chamber wherein RH was varied using humidifier (BioAire Lifestyle) and continuously monitored using a digital hygrometer (RS PRO RS-91, ± 3% RH Accuracy, 100% RH Max). Impedance spectroscopy was measured using impedance analyser (Autolab - Potentiostat/Galvanostat, Metrohm). An AC sinusoidal perturbation of 50 mV and a DC bias voltage of 0.5 V was applied over the frequency range 0.1 Hz to 1 MHz. Measurements were conducted using a precision source/measure unit (B2902A, Keysight-Agilent). Conductivity was calculated using the value of resistance obtained by EIS data fitting. The experimental conditions under which these measurements were performed for conductivity calculation were: (RH =100%) for fibre device having a single channel length of 100 μm, and (RH = 80%) for fibre devices with multiple channels of 10 μm in length over a length of 3.5 mm. For temperature dependent conductivity experiment device was kept under at RH = 90%. FET characteristics of the device was measured at RH of 44%, 66%, 77% and 88%. The time delay parameters (0.25 sec) were used for data presented in Figures 5D–5F (delay 0.05 sec). Cyclic voltammetry was performed in a three-electrode configuration. Slime film was coated on the Au electrode immersed a buffer (water) that served as the working electrode, a platinum wire served as the counter electrode, and a silver/silver chloride electrode served as the reference electrode. For pH dependent measurements, the pH of the Milli-Q water was adjusted by adding hydrochloric acid to it. The kinetic isotope measurements were conducted by saturating the sample with water (H_2O) and deuterated water (D_2O). Devices were held for 10 min before the measurements.

Optical and physical characterization of films

FTIR spectra of the dry and hydrated slime were acquired using the attenuated total reflection (ATR) technique (Bruker spectrometer). Dry slime flake (hydrate for 20 seconds) was pressed onto the ATR crystal for which 64 interferograms were accumulated at a spectral resolution of 4 cm^{-1}. Optical reflectance spectra were measured using Avaspec ULS2048 spectrometer (Avantes, grating 200−1100 nm), coupled to the Zeiss A1 upright microscope.

QUANTIFICATION AND STATISTICAL ANALYSIS

EIS spectrum analyser software was used for EIS data analysis and ImageJ software was used to calculate the area of fibres.